nature portfolio

https://doi.org/10.1038/s41557-022-00965-6

Supplementary information

Low-temperature liquid platinum catalyst

In the format provided by the authors and unedited

Supplementary Information

Low Temperature Liquid Platinum Catalyst

Md. Arifur Rahim[1]*, Jianbo Tang[1], Andrew J. Christofferson[2,3], Priyank V. Kumar[1], Nastaran Meftahi[2,3], Franco Centurion[1], Zhenbang Cao[1], Junma Tang[1], Mahroo Baharfar[1], Mohannad Mayyas[1], Francois-Marie Allioux[1], Pramod Koshy[4], Torben Daeneke[5], Christopher F. McConville[2,6], Richard B. Kaner[7,8], Salvy P. Russo[2,3], Kourosh Kalantar-Zadeh[1]*

Affiliations

[1]School of Chemical Engineering, University of New South Wales (UNSW), Sydney, New South Wales, Australia

[2]School of Science, STEM College, RMIT University, Melbourne, Victoria, Australia

[3]ARC Centre of Excellence in Exciton Science, School of Science, RMIT University, Melbourne, Victoria, Australia

[4]School of Materials Science and Engineering, University of New South Wales (UNSW), Sydney, New South Wales, Australia

[5]School of Engineering, RMIT University, Melbourne, Victoria, Australia

[6]Institute for Frontier Materials, Deakin University (Warren Ponds Campus), Geelong, Victoria, Australia.

[7]Department of Chemistry and Biochemistry, University of California, Los Angeles (UCLA), Los Angeles, CA, USA

[8]Department of Materials Science and Engineering, and California NanoSystems Institute, University of California, Los Angeles (UCLA), Los Angeles, CA, USA

*Corresponding authors. Email: ma.rahim@unsw.edu.au, k.kalantar-zadeh@unsw.edu.au

Contents

Supplementary Methods

Materials

Gallium (Ga, ingots, 99.9%) was purchased from Rotometals, USA. Platinum (Pt, solid beads of 1-3 mm, 99.9% purity) was purchased from Ezzi Vision, Australia. Pyrogallol (PG), acetic acid, dimethyl sulfoxide (DMSO), 3,3′,5,5′-tetramethylbenzidine (TMB), methylene blue (MB), methanol (CH_3OH), ascorbic acid, potassium hydroxide (KOH), sodium acetate, nitric acid (HNO_3) and hydrochloric acid (HCl) were purchased from Sigma-Aldrich and used as received. High-purity (Milli-Q) H_2O with a resistivity of 18.2 MΩ.cm was obtained from an inline Millipore RiOs/Origin H_2O purification system.

Characterisation

The UV-Vis absorption spectra were recorded on a Cary 5000 (PerkinElmer) spectrophotometer. X-ray photoelectron spectroscopy (XPS) was performed on an ESCALAB250Xi spectrometer (Thermo Scientific, UK). The incident radiation was monochromatic Al Kα X-rays (1486.68 eV) at 120W (13.8 kV × 8.7 mA). Survey (wide) and high resolution (narrow) scans were taken at analyzer pass energies of 100 eV and 20 eV, respectively. Base pressure in the analysis chamber was below 2.0×10^{-9} mbar. The temperature in the chamber was maintained at -50 °C to avoid liquefaction of the samples. The samples were etched for 2 min to remove any oxide layer. All data were processed using Advantage software and the energy calibration was referenced to the C 1s peak at 284.8 eV. Inductively coupled plasma-mass-spectrometry (ICP-MS) analyses were performed on a Nexion5000 (PerkinElmer, USA). The samples were prepared by dissolving a known amount the Ga-Pt samples (equilibrated at different temperature) in aqua regia (a mixture of HNO_3 and HCl with a molar ratio of 1:3) at 80 °C. Contact angle measurements were performed by a home-built set up using a cell phone with an attached macro lens. The Ga-Pt droplet (~10 μL)

was taken out from the stock and directly put in the aqueous solutions of different pH values. Raman spectroscopy was performed on an inVia Raman microscope (RENISHAW) with a 532 nm laser source, and the laser power was 10% with a 10 s exposure time.

MD simulations

Classical MD simulations were performed using the MD code LAMMPS[1] to generate a random configuration of 16 Pt in 112 Ga in a 13.4 × 13.4 × 13.4 $Å^3$ box. Sigma and epsilon values for Pt were 2.515 Å and 3.41 kcal/mol, respectively, while force field parameters for Ga were taken from our previous work[2]. The same procedure was used to generate configurations of 2 Pt in 198 Ga in a 15.6 × 15.6 × 15.6 $Å^3$ box. Bulk *ab initio* MD (AIMD) simulations were carried out in the Vienna ab initio Simulation Package (VASP)[3,4] at 318 K using the projector-augmented wave (PAW)[5] method, the PBE exchange correlation functional, an energy cut-off of 250 eV, and a 3 × 3 × 3 k-point grid. For interfacial systems, a 15 Å vacuum spacer was added in the *z* direction, and a 3 × 3 × 1 k-point grid was used. For the investigation of the oxidation of pyrogallol (PG), the PG and an O_2 molecule were added to the interfacial system after 50 ps of AIMD and positioned with the oxygens within ~3 Å of either interfacial Pt or Ga, with the energy cut-off increased to 500 eV and the timestep reduced from 1 fs to 0.5 fs. Additional PG oxidation investigations were performed by changing all but two, or one, interfacial Pt to Ga. From the single-Pt system, additional PG oxidation investigations were performed by changing the Pt to Ga, In, Bi, Sn, and Pd without relaxing the geometry, and with a geometry relaxation of 2 ps of AIMD before adding the PG and O_2. A partially oxidized interface was created by adding 6 O_2 molecules to the system of 1 Pt in 127 Ga. Calculations of self-diffusion coefficients were carried out on systems comprising 127 Ga and 1 Pt, with settings corresponding to the bulk simulations described above, run for 50 ps in triplicate. All analysis was performed using VMD 1.9.3.[6,7].

DFT calculations

DFT calculations were carried out using the VASP code. The PAW method and the PBE exchange-correlation functional are used. The wavefunctions were expanded with a kinetic energy cut-off value of 450 eV and converged k-grids were used. Structural relaxation was completed when the residual forces on atoms were less than 0.03 eV/Å. We performed mechanistic investigations of methanol oxidation on a liquid Ga slab measuring 9.048 Å x 9.048 Å, which contained four atomic layers (8 atoms/layer). To model the effect of Pt dopant, one of the surface Ga atoms was replaced with a Pt atom. More structural details of the slab and how they are generated can be found elsewhere[8]. A vacuum region greater than 10 Å in the direction normal to the slab is considered to avoid interactions between periodic images. For computing the potential energy diagram of PG oxidation on Ga and Ga-Pt surfaces, we utilized the snapshots from our AIMD simulations. Specific adsorbate configurations for PG oxidation were relaxed using DFT. The parameters used in our DFT calculations are the same as what we use for methanol oxidation.

Supplementary Figures 1–19

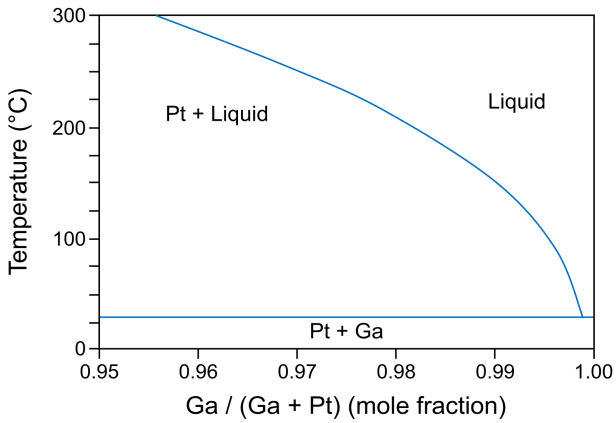

Figure 1. Phase diagram of binary Pt-Ga system in the temperature range of 0 to 300 °C, drawn using[9] FactSage 8.0.

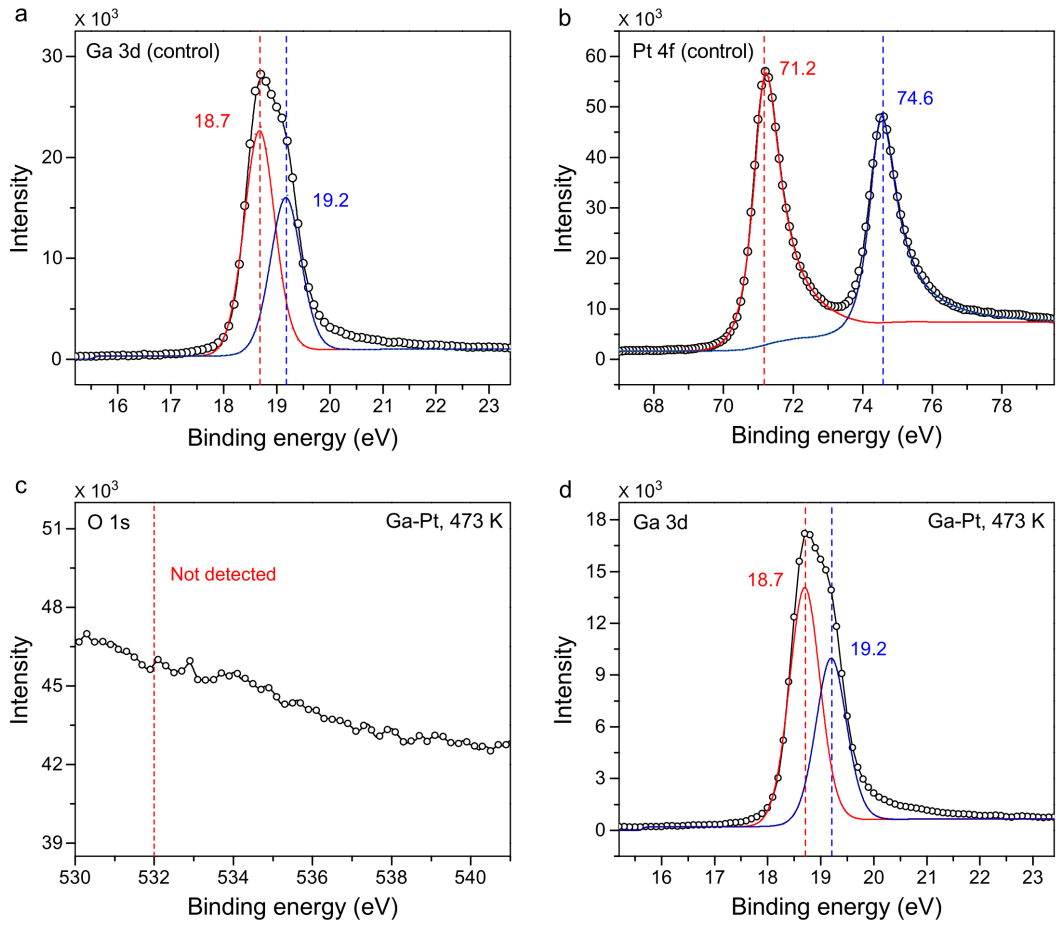

Figure 2. a, XPS spectra showing the Ga 3d region of a pure Ga sample (without Pt). **b**, XPS spectra showing the Pt 4f region of a pure Pt bead. **c**, XPS spectra showing the absence of oxygen in the Ga-Pt sample. **d**, XPS spectra showing the Ga 3d region of the Ga-Pt sample. No peak shift was observed for the Ga3d spectra comparing Ga-Pt and Ga (control) samples, possibly because of the ultra-low amount of dissolved Pt.

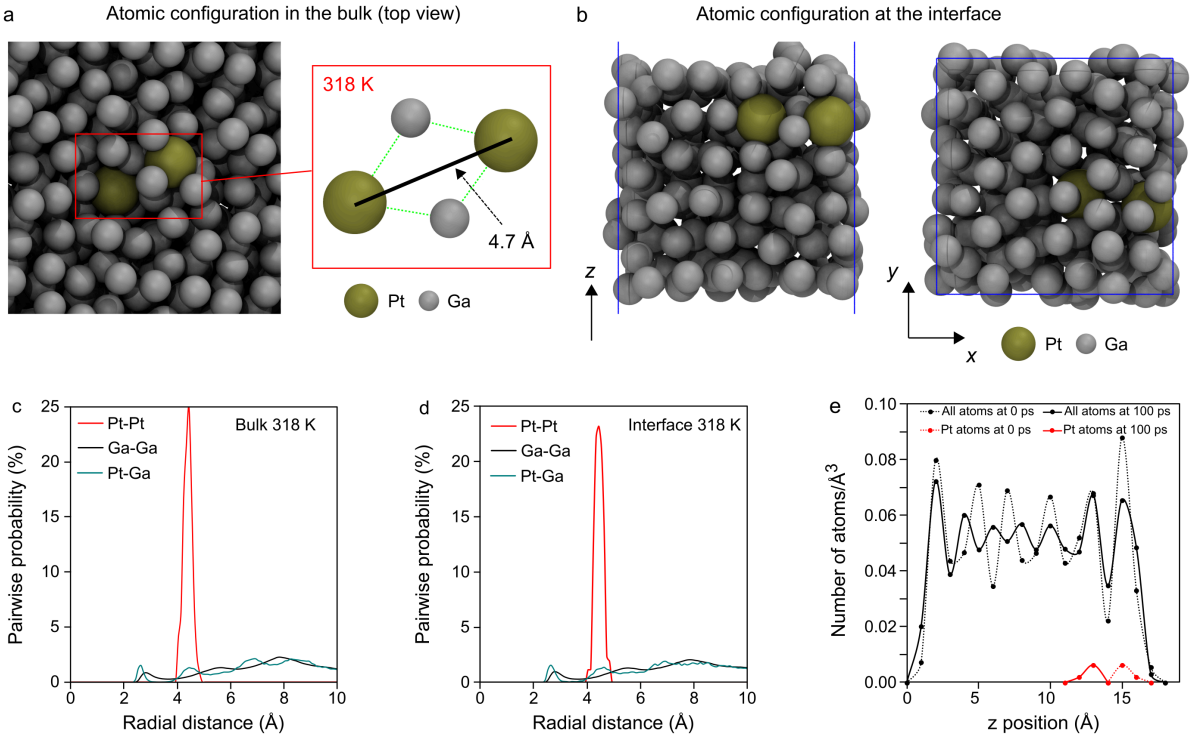

Figure 3. a,**b**, Representative snapshots of the atomic configurations of Pt in Ga (this system is constructed with 198 Ga atoms and 2 Pt atoms) in the bulk and at an interface, respectively. **c**,**d**, Pairwise probability function for Pt and Ga in the bulk and at an interface, respectively. **e**, Atomic density distribution for all atoms and Pt only as a function of *z* position for the interfacial system at 0 and 100 ps.

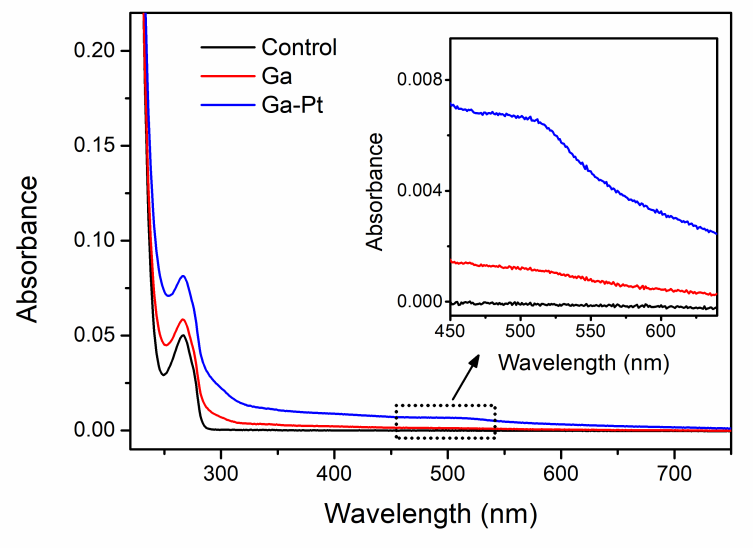

Figure 4. Catalytic PG oxidation over Ga and Ga-Pt systems at pH 2.8 after 24 h of reaction.

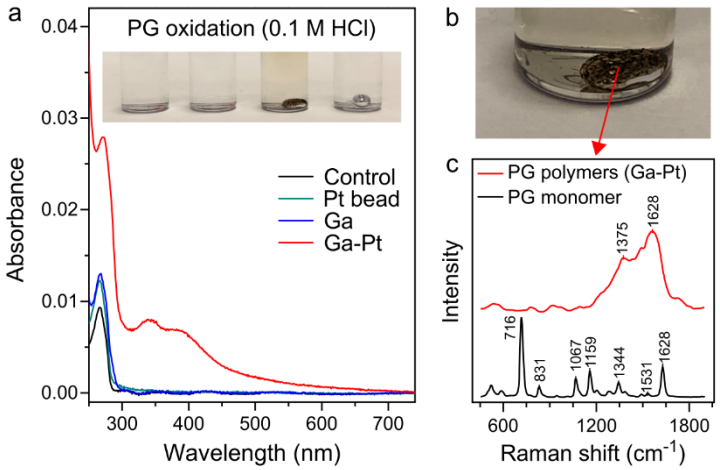

Figure 5. The oxidation of PG in 0.1 M HCl (pH 1). **a**, UV-Vis absorption spectra of the solution after 24 h of reaction. **b**, Along with the oxidation, a significant amount of polymers was observed to be deposited on the surface of the Ga-Pt droplet. **c**, The corresponding Raman spectra of the deposited PG polymers in comparison with PG monomer.

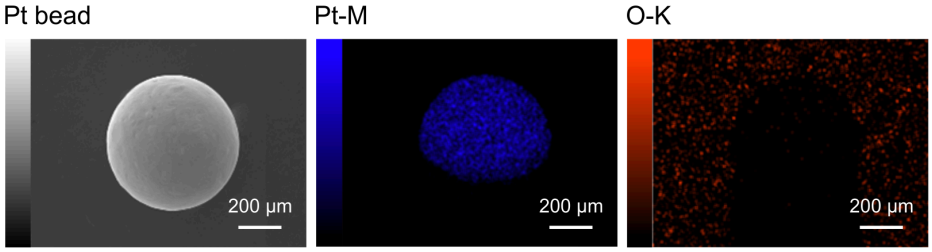

Figure 6. The SEM image of a representative Pt bead and the corresponding EDX mapping.

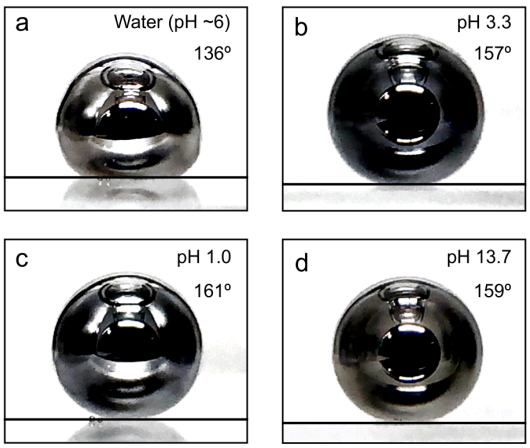

Figure 7. Contact angle measurements of a Ga-Pt droplet (~10 µL) on a quartz surface in acidic or basic conditions.

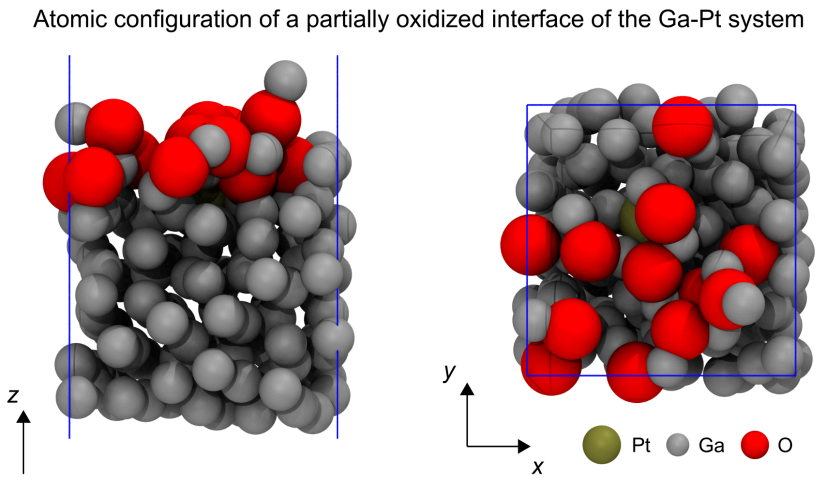

Figure 8. Partial oxidation of the Ga-Pt interface. Representative snapshot of the atomic configurations of the Ga-Pt interface (127 Ga, one Pt) oxidized by six O_2 molecules.

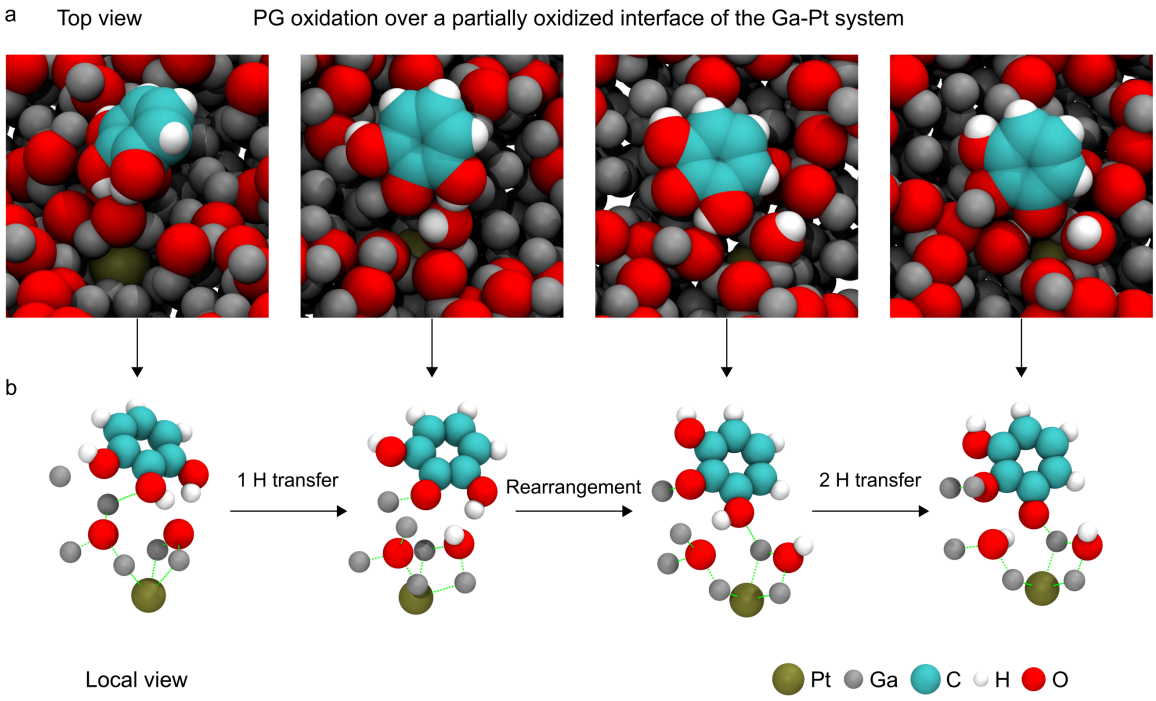

Figure 9. Oxidation of PG over partially oxidized Ga-Pt catalysts. **a**, Top view. **b**, Local view (showing the different steps of the oxidation reaction).

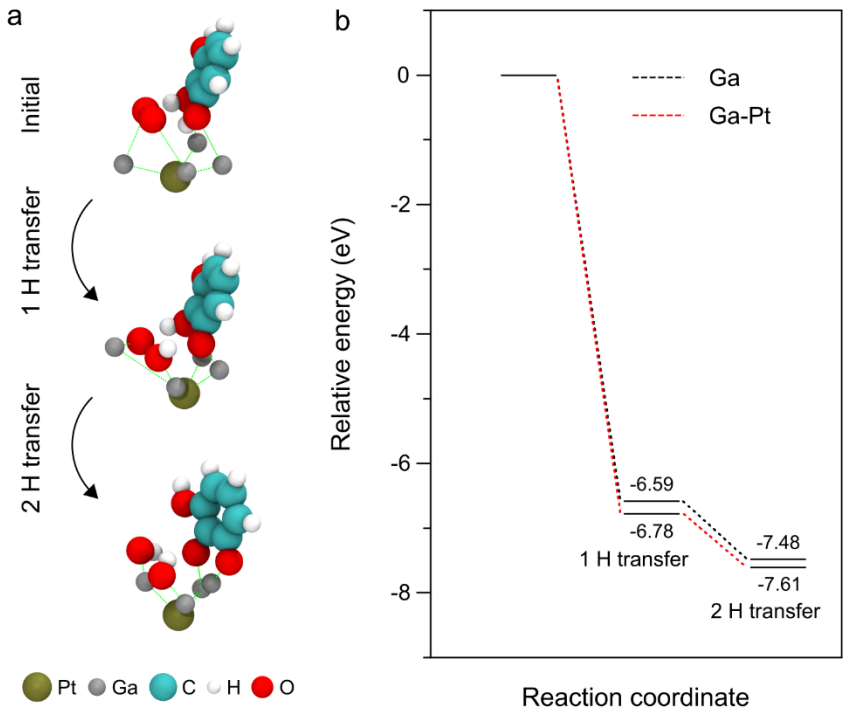

Figure 10. DFT calculations for the oxidation of PG over Ga-Pt catalysts. **a**, local view and **b**, energy diagram.

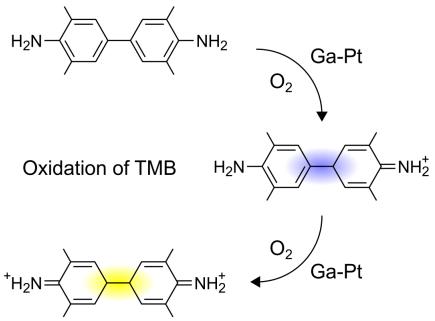

Figure 11. General reaction mechanism for the catalytic oxidation of TMB.

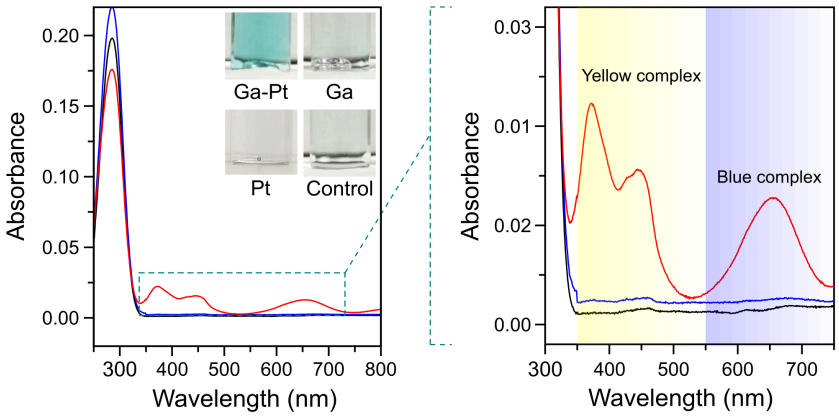

Figure 12. Absorption spectra showing the TMB oxidation over Ga, Ga-Pt and Pt catalysts and their corresponding photographs. A magnified region of the absorption spectra clearly showing the difference in activity of Ga, Ga-Pt and Pt catalysts for TMB oxidation.

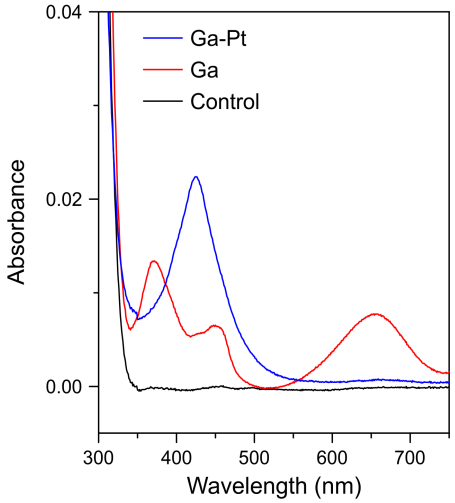

Figure 13. Absorption spectra showing the TMB oxidation over Ga and Ga-Pt catalysts, and the corresponding control after 72 h of reaction.

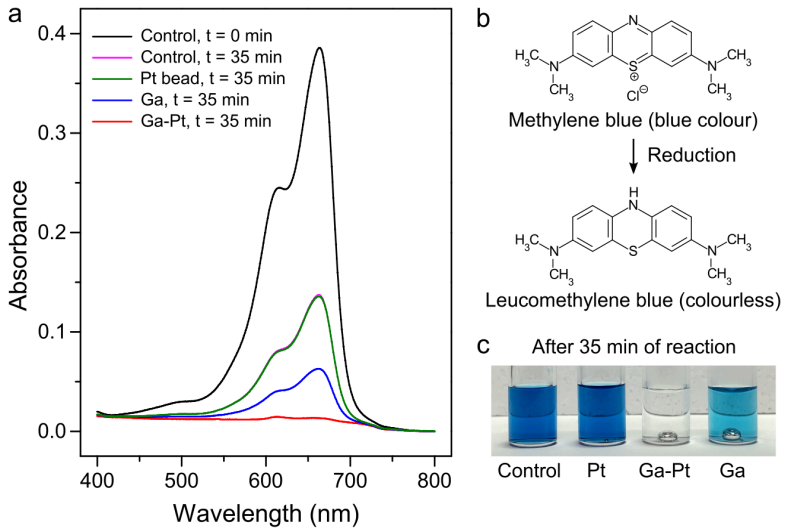

Figure 14. The reduction of MB in 0.1 M HCl (pH 1) and ascorbic acid as a reducing agent. **a**, UV-Vis absorption spectra of the solution after 35 min of reaction. **b**, The reduction pathway for the conversion of MB (coloured) to Leuco-MB (colourless). **c**, The corresponding photographs showing the activity of different catalysts.

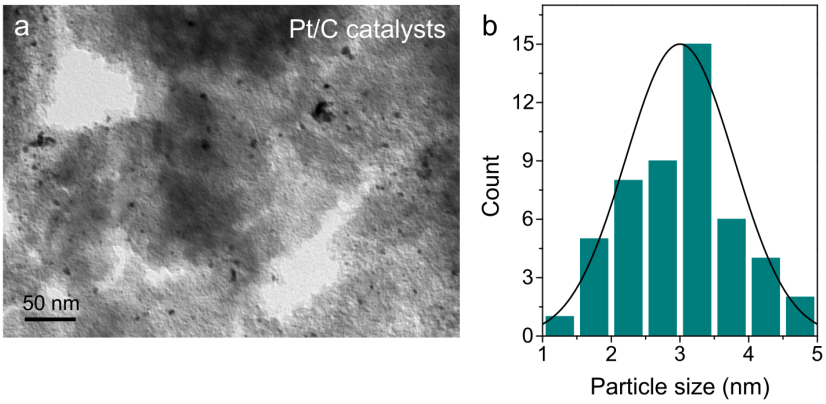

Figure 15. a, TEM image of the commercial Pt/C catalyst and **b**, the corresponding histogram of the particle size used in this study.

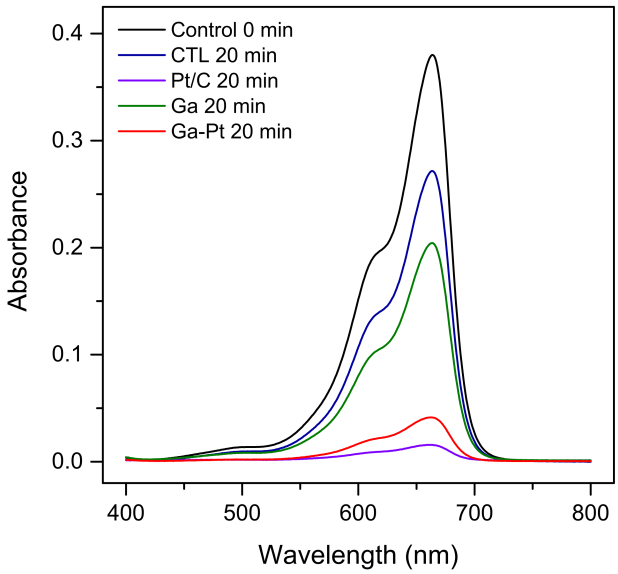

Figure 16. Comparison of Ga-Pt and Pt/C (10 wt% Pt) for the reduction of MB in 0.1 M HCl (pH 1) and ascorbic acid as a reducing agent. UV-Vis absorption spectra of the solution after 25 min of reaction.

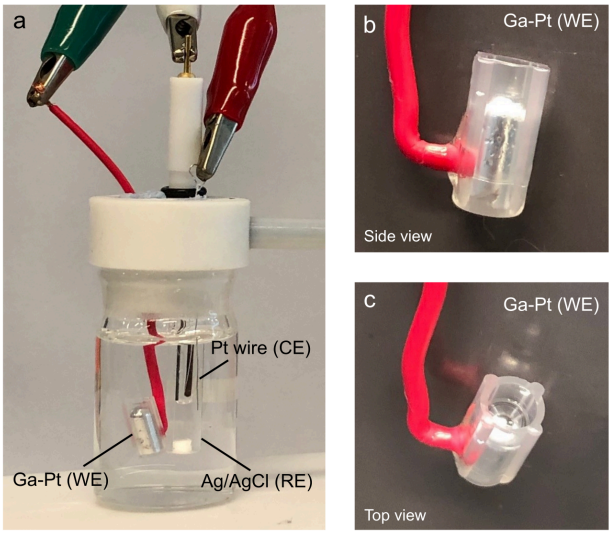

Figure 17. The electrochemical set up used in this study. **a**, The overall three electrode setup. **b**, Side view and **c**, top view of the working electrode (WE).

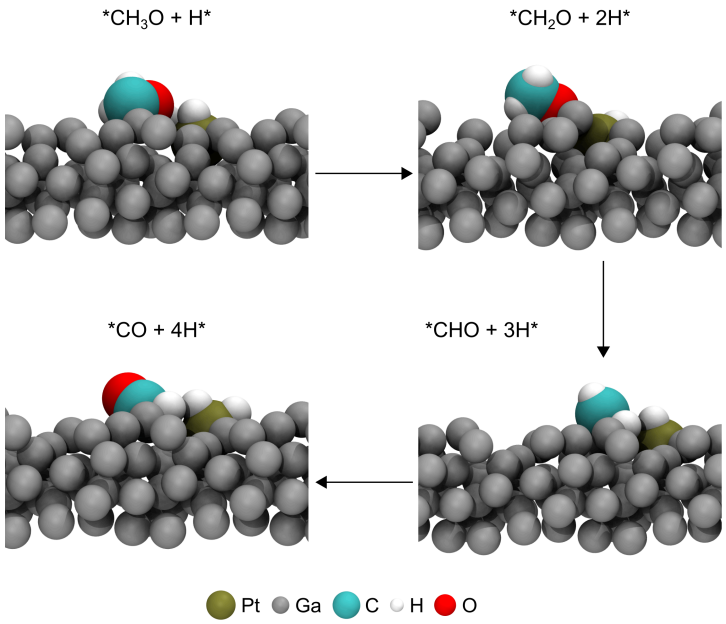

Figure 18. DFT snapshots (side-view) of methanol oxidation over Ga-Pt surface.

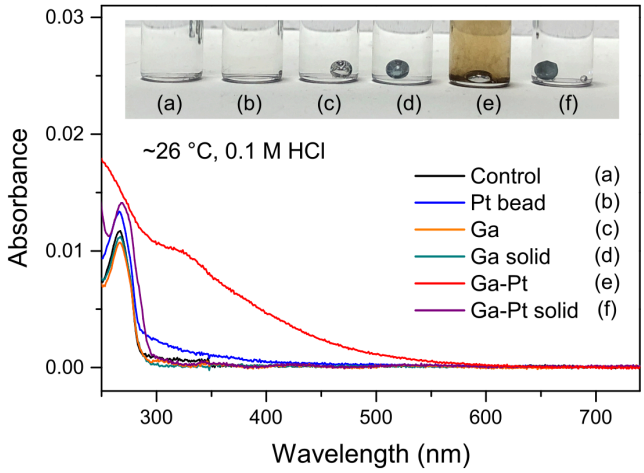

Figure 19. Comparison of solid Ga-Pt and liquid Ga-Pt for the oxidation of PG (0.1 mg mL^{-1}, 0.1 M HCl) at ~26 °C, after 12 days of reaction.

Supplementary Tables

Table 1. Comparison of other metals in the Ga matrix toward PG oxidation

	H transfer from PG to O_2		
Single atom	**System not relaxed**	**System relaxed for 2 ps before adding PG and O_2**	**Single atom position at the relaxed interface**
Pt	Both H transferred	Both H transferred	Slightly embedded
Ga	1 H transferred	1 H transferred	n/a
In	Both H transferred	Both H transferred	Slightly embedded
Bi	Both H transferred	1 H transferred	Protruding
Sn	Both H transferred	1 H transferred	Protruding
Pd	Both H transferred	No H transferred	Deeply embedded

Table 2. Catalytic activity of different materials for methanol oxidation

System	Mass activity (MeOH oxidation) mA mg^{-1}_{Pt}	Reported in comparison with	Reference
Pt/C (20 wt%)	~1.01×10^3	NA	10
Pt–nickel hydroxide–graphene	~1.23×10^3	Pt/C (20 wt%)	10
Pt/rGO	~1.07×10^3	Pt/C (20 wt%)	10
Pt_1/RuO_2	~6.76×10^3	Pt/C (20 wt%)	11
p-Pt_1Cu_1/AP-GNPs[a]	~3.6×10^3	Pt/C (20 wt%)	12
PtCu-O EONDs[b]	~4.43×10^3	Pt/C (20 wt%)	13
PtCu nanoflowers	~2.26×10^3	Pt/C (20 wt%)	14
Ga-Pt	~1.8×10^7	Compared with reported values of different catalysts listed here	This work

[a]1-aminopyrene functionalized graphene nanoplates

[b]Excavated octahedral nanostructures built from nanodendrites (EONDs)

Supplementary Notes

Note 1. Determination of surface Pt atoms

Ga-Pt droplet

This calculation based on the assumption that the Ga-Pt droplet is a smooth sphere with negligible density change (in comparison to Ga) due to the small amount of dissolved Pt. The number of surface Pt atoms was considered to be statistically constant over time as the number of Pt atoms moving vertically to and away from the surface are mutually compensated. The surface area $S_{droplet}$ (m^2) of the Ga-Pt droplet can be written as:

$$S_{droplet} = 4\pi r_{droplet}^2 \quad \text{(S1)}$$

where $r_{droplet}$ is the radius of the spherical Ga-Pt droplet of 40 µL and equals to 2.12×10^{-3} m. Assuming an optimal close-packing of the Ga atoms on a two-dimensional surface plane, the fractional filling efficiency ($f_{surface}$) is 0.91 for spheres or ellipses[15,16]. Therefore, the total surface area $S'_{droplet}$ (m^2) of all Ga atoms on the surface can be written as:

$$S'_{droplet} = 0.91\, S_{droplet} \quad \text{(S2)}$$

The cross-sectional area α_{Ga} (m^2) of a Ga atom can be written as:

$$\alpha_{Ga} = \pi r_{Ga}^2 \quad \text{(S3)}$$

where r_{Ga} is the atomic radius of a Ga atom and equals to 135 pm[17]. Therefore, the number of Ga atoms (N_{Ga}) on the surface of the Ga-Pt droplet is calculated to be $N_{Ga} = S'_{droplet} / \alpha_{Ga} = 8.97 \times 10^{14}$.

The temperature-dependent solubility (S_T) of Pt (Fig. 1b) in Ga is 5.84×10^{-5} (at%) and 8.13×10^{-5} (at%) at 45 and 55 °C, respectively. Therefore, the number of surface Pt atoms (N_{Pt}) on the Ga-Pt droplet is estimated to be $N_{Pt\text{-}45} = N_{Ga} \times S_{45} = 5.23 \times 10^{10}$ and $N_{Pt\text{-}55} = N_{Ga} \times S_{55} = 7.29 \times 10^{10}$ at 45 and 55 °C, respectively.

Pt bead

This calculation is based on the assumption that the Pt bead (Supplementary Fig. 6) is a solid and smooth sphere of radius ~0.3 mm. Therefore, the surface area of the Pt bead $S_{Pt\text{-}bead}$ = 1.13 × 10^{-6} m^2 and $S'_{Pt\text{-}bead}$ = 1.03 × 10^{-6} m^2 according to Eq. S1 and Eq. S2, respectively. According to Eq. S3, the cross-sectional area (α_{Pt}) of a Pt atom (atomic radius of a Pt atom r_{Pt} = 138.5 pm)[17] is calculated to be α_{Pt} = 6.03 × 10^{-20} m^2. Therefore, the number of Pt atoms on the surface of the Pt bead ($N_{Pt\text{-}bead}$) is $N_{Pt\text{-}bead} = S'_{Pt\text{-}bead} / \alpha_{Pt}$ = 1.71 × 10^{13}.

Ratio of surface Pt atoms (Ga-Pt *vs* Pt bead)

Form the above calculations the ratio of surface Pt atoms can be estimated as (for PG oxidation):

$$\frac{Pt_{Ga-Pt}}{Pt_{bead}} = \frac{N_{Pt-45}/S_{droplet}}{N_{Pt-bead}/S_{Pt-bead}} = 6.17 \times 10^{-5} \quad \text{(S4)}$$

Note that for the activity comparison, the contribution from Ga (control) was deducted from the contribution of Ga-Pt system to obtain the liquid Pt specific contribution.

Pt/C catalyst

The commercial Pt/C catalyst used in this study, contains 10 wt% of Pt. Therefore, the total mass of Pt in a 1 mg of Pt/C catalyst is 0.1 mg (used for the comparison tests for the MB reduction). Pt/C catalyst contains Pt as a form of nanoparticles with a mean radius ($r_{Pt\text{-}NP}$) of ~1.5 nm. Hence, the volume $V_{Pt\text{-}NP}$ (m^3) of each Pt NP can be written as:

$$V_{Pt-NP} = \frac{4}{3}\pi r_{Pt-NP}^3 \quad \text{(S5)}$$

Considering the density of Pt (ρ)[17] as 21.46 g/cm^3, the mass of each Pt NP $m_{Pt\text{-}NP}$ (g) is calculated to be $m_{Pt\text{-}NP} = \rho V_{Pt\text{-}NP}$ = 3.03 × 10^{-19} g. Therefore, the number of Pt NP ($N_{Pt\text{-}NP}$) in 1 mg of Pt/C (i.e., 0.1 mg of Pt) is $N_{Pt\text{-}NP}$ = 3.30 × 10^{14}.

The surface area of each Pt NP $S_{Pt\text{-}NP} = 2.83 \times 10^{-17}$ m^2 and $S'_{Pt\text{-}NP} = 2.57 \times 10^{-17}$ m^2 according to Eq. S1 and Eq. S2, respectively. Therefore, the number of Pt atoms on the surface of each Pt NP ($N_{Pt(Pt\text{-}NP)}$) is calculated to be $N_{Pt(Pt\text{-}NP)} = S'_{Pt\text{-}NP} / \alpha_{Pt} = 4.27 \times 10^2$. Hence, the total number of surface Pt atoms in 1 mg of Pt/C (*i.e.*, 0.1 mg of Pt) catalyst ($N_{Pt(Pt/C\text{-}total)}$) is calculated to be $N_{Pt(Pt/C\text{-}total)} = 1.40 \times 10^{17}$.

Ratio of surface Pt atoms (Ga-Pt *vs* Pt/C)

Form the above calculations the total surface area of the Pt NP ($S_{Pt\text{-}NP\text{-}total}$) in Pt/C is calculated to be $S_{Pt\text{-}NP\text{-}total} = S_{Pt\text{-}NP} \times N_{Pt\text{-}NP} = 9.34 \times 10^{-3}$ m^2. Therefore, the ratio of surface Pt atoms for Ga-Pt ($Pt_{Ga\text{-}Pt}$) and Pt/C ($Pt_{Pt/C}$) can be estimated as (for MB reduction):

$$\frac{Pt_{Ga-Pt}}{Pt_{Pt/C}} = \frac{N_{Pt-55}/S_{droplet}}{N_{Pt(Pt/C-total)}/S_{Pt-NP-total}} = 8.61 \times 10^{-5} \quad \text{(S6)}$$

Note that for the activity comparison (for MB reduction), the contribution from Ga (control) was deducted from the contribution of Ga-Pt system to obtain the liquid Pt specific contribution.

Ga-Pt electrode

This calculation based on the assumption that the Ga-Pt electrode is of cylindrical shape with negligible density change (compared to Ga) due to the small amount of dissolved Pt. The number of surface Pt atoms was considered to be statistically constant over time as the number of Pt atoms moving vertically to and away from the surface are mutually compensated. The radius (r_{el}) of the Ga-Pt electrode is 2×10^{-3} m. Given the $f_{surface} = 0.91$ for an optimal close-packing of the Ga atoms, the total surface area of all Ga atoms on the electrode surface S'_{el} (m^2) can be written as (Eq. 1 and Eq. 2):

$$S'_{el} = 0.91 \times \pi r_{el}^2 \quad \text{(S7)}$$

The number of Ga atoms on the surface of the Ga-Pt electrode ($N_{Ga\text{-}el}$) is estimated to be $N_{Ga\text{-}el} = S'_{el} / \alpha_{Ga} = 1.99 \times 10^{14}$. Using the solubility of Pt in Ga, $S_{70} = 2.17 \times 10^{-4}$ (at%) at 70 °C

(Figure 1b), the number of surface Pt atoms on the Ga-Pt electrode is estimated to be $N_{Pt} = N_{Ga\text{-}el} \times S_{70} = 4.31 \times 10^{10}$.

Note that, this number of Pt atoms are equivalent to 1.39×10^{-8} mg, which is used to estimate the mass activity for methanol oxidation. After deducting the contribution from Ga for the Ga-Pt system, the peak current output was ~0.4 mA. Therefore, the mass activity is 2.80×10^{7} mA mg^{-1}_{Pt}.

Lateral diffusion length of Pt in Ga-Pt

Considering only the lateral diffusion of the Pt atoms in Ga-Pt, the lateral diffusion length L_d (m) of each Pt atom can be estimated by the following equation:

$$L_d = \sqrt{4Dt} \tag{S8}$$

where 4 is a dimensional constant for two dimensions, D is the lateral diffusion coefficient of a Pt atom in the Ga matrix (obtained from simulation) and equals to 1.5×10^{-10} m^2. Considering a time of 1 s, L_d is estimated to be $L_d = 2.45 \times 10^{-5}$. Given that the diameter of a Pt atom is $2r_{Pt}$ = 277 pm, the number of new positions (in the 1 s considered) is approximated to be $P_{Pt} = L_d / 2r_{pt} = 8.84 \times 10^{4}$.

Note 2. The aspect of oxide formation

Since the Ga-oxide skin is amphoteric in nature, according to the Pourbaix diagram and previous experimental observations[18-20], the oxide layer can be removed at pH ~3 and lower or pH ~10 and above. For the Ga-Pt system, we also investigated such oxide layer formation in both high and low pH environments. As it is well known that the presence of surface oxide alters the overall surface adhesion[18,19], we performed contact angle (CA) measurements of a liquid Ga-Pt droplet in different pH values (Supplementary Fig. 7). While the Ga-Pt droplet in water showed an oxidized surface with a CA of 136°, the same droplet at different pH (3.3, 1.0 and 13.7) showed a similar CA around 160°, suggesting that the surface oxide formation is

negligible in these conditions[18,19]. Based on the above evidence, we additionally performed the PG oxidation reaction at pH 1 (0.1 M HCl) where we could safely assume the absence of an oxide layer (Supplementary Fig. 5). To further corroborate, we also carried out a reduction reaction at pH 1 (0.1 M HCl), where the presence of an oxide interface would also be negligible due the low pH and a reducing environment (MB reduction, Fig. 4b). Again, in these additional tests, the catalytic activity from the Ga-Pt system was observed to be remarkably higher than the other systems.

As it may not be entirely possible to rule out the presence of transient local oxidized interfaces, we further investigated the PG oxidation over a partially oxidized surface of the Ga-Pt system using AIMD. The atomic configuration of such an interface is presented in Supplementary Fig. 8. To test whether the oxidation of PG can still occur at a partially oxidized interface, six O_2 molecules were added to the system of 127 Ga and one Pt and equilibrated before adding PG. Following the addition of PG, the oxidation occurred in a similar manner to the reaction described previously, where it was necessary for at least one of the PG oxygens to be adjacent to a Ga atom in direct contact with the Pt in order for the H to be transferred (Supplementary Fig. 9). The simulations also indicate that a significant rearrangement of the interfacial Ga atoms in contact with the Pt occurs during the oxidation process, which necessitates a fully liquid interface. We note that the local transient oxide layer should disappear in low or high pH environment (according to the CA measurements and the observation that the catalytic activity of the Ga-Pt at pH 1) and should not influence significantly to the overall catalytic performance of the Ga-Pt system due to its transient, local presence.

References

1. S. Plimpton, *J. Comput. Phys.* **117**, 1-19 (1995).
2. J. Tang *et al.*, *Nat. Nanotechnol.* **16**, 431-439 (2021).
3. G. Kresse, J. Furthmüller, *Phys. Rev. B* **54**, 11169-11186 (1996).
4. G. Kresse, D. Joubert *Phys. Rev. B* **59**, 1758-1775 (1999).
5. P. E. Blöchl, *Phys. Rev. B* **50**, 17953-17979 (1994).
6. W. Humphrey, A. Dalke, K. Schulten, *J. Mol. Graphics* **14**, 33-38 (1996).7. T. Giorgino, *Journal of Open Source Software* **4**, 1698 (2019).
8. M. Mayyas *et al.*, *Adv. Mater.* 32, 2001997 (2020).
9. C. W. Bale *et al.*, *Calphad* **54**, 35-53 (2016).
10. Huang, W. *et al. Nat. Commun.* **6,** 10035 (2015).
11. Zhang, Z. *et al. Nat. Commun.* **12,** 5235 (2021).
12. Zhang, G. *et al. J. Mater. Chem. A* **4,** 3316-3323 (2016).
13. Wu, F. *et al. J. Mater. Chem. A* **7,** 8568-8572 (2019).
14. Zhang, Z. *et al. Adv. Mater.* **28,** 8712-8717 (2016).
15. Jiao, X. *et al. Phys. Chem. Chem. Phys.* **19,** 13547-13552 (2017).
16. Matsumoto, T. & Nowacki, W. *Zeitschrift für Kristallographie - Crystalline Materials* **123,** 401-421 (1966).
17. Haynes, W. M., CRC Handbook of Chemistry and Physics, 97th Edition. CRC Press: 2016.
18. Dickey, M. D. *ACS Appl. Mater. Interfaces* **6,** 18369-18379 (2014).
19. Bilodeau, R.A., Zemlyanov, D. Y. & Kramer, R. K. *Adv. Mater. Interfaces* **4,** 1600913 (2017).

20. Marcel Pourbaix, *Atlas Of Electrochemical Equilibria In Aqueous Solutions* (National Association of Corrosion Engineers, 1974).